Title

Imaging biomarkers of TERT or GABPB1 silencing in TERT-positive glioblastoma

Journal

Neuro-Oncology, 24(11)

ISSN

1522-8517

Authors

Minami, Noriaki
Hong, Donghyun
Stevers, Nicholas
et al.

Publication Date

2022-11-02

DOI

10.1093/neuonc/noac112

Peer reviewed

Neuro-Oncology
24(11), 1898–1910, 2022 | https://doi.org/10.1093/neuonc/noac112 | Advance Access date 23 April 2022

Imaging biomarkers of TERT or GABPB1 silencing in TERT-positive glioblastoma

Noriaki Minami[†], Donghyun Hong[†], Nicholas Stevers, Carter J. Barger, Marina Radoul, Chibo Hong, Lee Chen, Yaewon Kim, Georgios Batsios, Anne Marie Gillespie, Russel O. Pieper, Joseph F. Costello, Pavithra Viswanath, and Sabrina M. Ronen

Department of Radiology and Biomedical Imaging, University of California, San Francisco, California, USA (N.M., D.H., M.R., Y.K., G.B., A.M.G., P.V., S.M.R.); Department of Neurological Surgery, University of California, San Francisco, California, USA (N.S., C.J.B., C.H., L.C., R.O.P., J.F.C.)

Corresponding Author: Sabrina M. Ronen, PhD, University of California San Francisco, 1700 4th Street, San Francisco, CA 94158, USA (sabrina.ronen@ucsf.edu).

[†]These authors contributed equally to this work.

Abstract

Background. *TERT* promoter mutations are observed in 80% of wild-type IDH glioblastoma (GBM). Moreover, the upstream *TERT* transcription factor GABPB1 was recently identified as a cancer-specific therapeutic target for tumors harboring a *TERT* promoter mutation. In that context, noninvasive imaging biomarkers are needed for the detection of TERT modulation.

Methods. Multiple GBM models were investigated as cells and in vivo tumors and the impact of TERT silencing, either directly or by targeting GABPB1, was determined using ^{1}H and hyperpolarized ^{13}C magnetic resonance spectroscopy (MRS). Changes in associated metabolic enzymes were also investigated.

Results. ^{1}H-MRS revealed that lactate and glutathione (GSH) were the most significantly altered metabolites when either TERT or GABPB1 was silenced, and lactate and GSH levels were correlated with cellular TERT expression. Consistent with the drop in lactate, ^{13}C-MRS showed that hyperpolarized [1-^{13}C]lactate production from [1-^{13}C]pyruvate was also reduced when TERT was silenced. Mechanistically, the reduction in GSH was associated with a reduction in pentose phosphate pathway flux, reduced activity of glucose-6-phosphate dehydrogenase, and reduced NADPH. The drop in lactate and hyperpolarized lactate were associated with reductions in glycolytic flux, NADH, and expression/activity of GLUT1, monocarboxylate transporters, and lactate dehydrogenase A.

Conclusions. Our study indicates that MRS-detectable GSH, lactate, and lactate production could serve as metabolic biomarkers of response to emerging TERT-targeted therapies for GBM with activating *TERT* promoter mutations. Importantly these biomarkers are readily translatable to the clinic, and thus could ultimately improve GBM patient management.

Key Points

- TERT silencing directly or via GABPB1 is detectable in GBM by MRS imaging.
- TERT silencing is linked to levels of glutathione, lactate, and lactate production.

To maintain limitless proliferation, cancer cells must activate telomere maintenance mechanisms that avoid telomere shortening during DNA replication.[1] Expression of telomerase reverse transcriptase (TERT) is the most common mechanism through which cancers maintain their telomere length and achieve immortality. Activating mutations in the *TERT* promoter is one mechanism by which TERT expression can be restored. Such mutations have been reported

Importance of the Study

TERT promoter mutations are observed in most GBM tumors and result in TERT expression, which is essential for tumor growth. Recent studies show that GABPB1, the upstream transcription factor of *TERT*, provides a promising tumor-specific therapeutic target. However, imaging methods that can detect TERT expression and its inhibition by emerging therapies are limited. Here, we show that TERT expression can be imaged noninvasively using magnetic resonance spectroscopy (MRS). Most notably, we report that ^{1}H-MRS-detectable levels of glutathione and lactate are correlated with TERT expression and that hyperpolarized ^{13}C-MRS-detectable lactate production from pyruvate is also reduced in TERT-silenced cells. Importantly metabolic imaging of glutathione, lactate, and hyperpolarized lactate has been performed in GBM patients. The metabolic imaging biomarkers identified in this study could therefore be readily translated to the clinic and thus improve the monitoring and personalized treatment of GBM patients.

in the majority of human cancers[2,3] and over 80% of primary wild type isocitrate dehydrogenase (IDH) glioblastoma (GBM) and mutant IDH oligodendroglioma patients harbor a *TERT* promoter mutation.[2,4]

TERT is therefore considered a potential therapeutic target.[5] Unfortunately, inhibiting TERT or telomerase is also detrimental to normal stem and germline cells, leading to challenges for telomerase-targeted therapy in the clinic.[6] However, recent findings demonstrate that the mutant *TERT* promoter provides a *de-novo* binding site for upstream E26 transformation-specific (ETS)-family transcription factors including GABP. GABP is thus recruited to the mutant *TERT* promoter to activate TERT expression in a tumor-specific manner.[7–10] As such, a subunit of GABP, namely GABPB1, is now considered a promising target for TERT inhibition and glioma treatment.

In this context, biomarkers of TERT are viewed as central for monitoring response to TERT-targeted therapies. *TERT* promoter mutations can be detected by genomic analysis.[11] However, this requires invasive tumor resection and is of limited clinical relevance for longitudinal monitoring of response to treatment. In contrast, imaging biomarkers that can detect TERT expression could provide a noninvasive means for monitoring TERT status.

Consensus magnetic resonance imaging (MRI) recommendations were recently established for brain tumor patients.[12] But these methods are generally unable to specifically detect molecular genetic events. However, recent studies have shown the utility of magnetic resonance spectroscopy (MRS) for detection of the metabolic reprogramming associated with molecular drivers of glioma.[13] For example, ^{1}H-MRS, which probes steady-state metabolites, can detect 2-hydroxyglutarate (2HG) reporting on IDH status.[14] It also detects elevated choline and lactate reflecting cell proliferation and the Warburg effect.[15,16] State-of-the-art hyperpolarized ^{13}C-MRS provides information regarding metabolic fluxes and has also been used to visualize the Warburg effect.[17–19] Concerning TERT imaging, we have identified ^{1}H and hyperpolarized ^{13}C-MRS-detectable metabolic changes associated with TERT in mutant IDH models.[20,21] However, to date, no studies have imaged the metabolic alterations associated with TERT in wild-type IDH GBM models. Here, we show that the major metabolic changes following TERT-silencing are a drop in ^{1}H-MRS-detectable glutathione (GSH) and lactate. We also found that the ^{13}C-MRS-detectable production of hyperpolarized lactate from pyruvate was lower when TERT was silenced. Importantly, our metabolic observations were comparable when TERT expression was silenced directly or via silencing of its upstream transcription factor GABPB1. Collectively, our findings point to potential translatable biomarkers of TERT inhibition by emerging therapeutics in wild-type IDH GBM.

Materials and Methods

See Supplementary Material for details.

Cell Models

TERT or GABPB1 silencing was investigated in immortalized normal human astrocytes NHA E6E7HRasV12hTERT (NHARas/TERT)[22] and U87 cells treated with RNA interference for TERT or GABPB1 using two nonoverlapping siRNA pools (Dharmacon, Supplementary Table S1). It was also investigated in U251, GBM1, and GS2-based models in which silencing was by shRNA transduction (U251shTERT-2, U251shTERT-3, U251shB1-2, U251shB1-1, GBM1shTERT-2, GBM1shTERT-3, GBM1shB1-2, GBM1shB1-1, GS2shCtrl, GS2shTERT-2, GS2shB1-2, Supplementary Table S2).[7] All lines were routinely tested for mycoplasma and authenticated by short tandem repeat fingerprinting within 6 months of study.

^{1}H-MRS. —Cells were extracted using dual-phase extraction.[23] The lyophilized aqueous phase was resuspended in 400 µL D_2O-based phosphate buffer with sodium 3-trimethylsilyl propionate-2,2,3,3-d4 (TSP) as an external reference. ^{1}H spectra were acquired using a 500 MHz Spectrometer (Bruker). Spectra were analyzed using MNOVA (Mestrelab Research). Metabolites were quantified by integration, corrected for saturation, and normalized to cell number and TSP.[24] SIMCA software was used for principal component analysis (PCA), orthogonal partial least discriminant analysis (OPLS-DA), and to determine Variable Importance in Projection (VIP) scores, which reveal the importance of each metabolite to group separation.[21,25]

^{13}C-MRS. —Cells cultured for 48 h in media with half the normal glucose replaced by [2-^{13}C]glucose were extracted and proton-decoupled ^{13}C-MRS spectra were recorded and analyzed as above. Peak integrals were corrected for saturation and NOE and normalized as above.[24]

RT-qPCR. —RNA was subjected to reverse transcription using high-capacity cDNA reverse transcription kit (Applied Biosystems). Real-time polymerase chain reaction (PCR) was performed using POWER SYBR Green Master Mix (Applied Biosystems) in a QuantStudio5. The abundance of each target mRNA was normalized to endogenous GUSB. For primer sequences, see Supplementary Table S3.

Spectrophotometric assays. —NAD$^+$/NADH and NADP$^+$/NADPH levels were measured using commercial kits (Biovision) with OD450nm measured using an INFINITE 200 microplate reader (TECAN). Reactive oxygen species (ROS) were measured using DCFDA/H2DCFDA–Cellular ROS assay (Abcam). Fluorescence was measured at Ex/Em + 485/535 nm.

Hyperpolarized ^{13}C-MRS. —3 to 8 × 10^7 cells in a 5 mm NMR tube were mixed with 6 µL of [1-^{13}C]pyruvate prepared as previously.[26] Spectra were acquired using a 500 MHz spectrometer (Agilent) using a 5° flip angle and 3s TR over 300s. Data were analyzed using MNOVA and normalized to maximum [1-^{13}C]pyruvate and cell number.

In vivo ^{1}H-MRS. —Animal studies were performed under UCSF Institutional Animal Care and Use Committee approval. 5 × 10^5 U251shCtrl, U251shTERT-2, U251shB1-2 cells were injected intracranially in 6–8 week old nu/nu rats. MR studies were performed using a 3T preclinical MR scanner (Biospec, Bruker). T_2-weighted images were acquired using a spin-echo-based TurboRARE sequence. Tumor volume was determined as previously.[27] ^{1}H single voxel spectroscopy was acquired from a 4 × 4 × 4mm^3 voxel using the PRESS sequence with TE = 16ms (TE1 = TE2 = 8 ms), TR = 2000 ms, averages = 512, 1024 data points, spectral bandwidth 1250 Hz. LCModel[28] was used to quantify the spectra.

In vivo hyperpolarized ^{13}C-MRS. —24 µL [1-^{13}C]pyruvate was polarized and injected via tail vein over 12s.[26] Spectra were acquired using a spectral-spatial echo-planar spectroscopic imaging (EPSI)[29] sequence (flip-angle = 30° for [1-^{13}C]lactate and 6° for [1-^{13}C]pyruvate), spatial resolution = 5.375 × 5.375 × 8 mm^3, temporal resolution = 3s, 20 repetitions, 256 data points). Spectral signal to noise was improved using Tensor denoising.[30] Spectra were processed using a custom-written Matlab script (https://github.com/donghyunh/2DEPSI_Analysis.git) and metabolites were quantified using area under the curve (AUC).

Statistical Analysis

All experiments were performed at least 3 times. Results are presented as mean ± standard deviation. Statistical significance was assessed in GraphPad Prism using an unpaired two-tailed Student's T-test assuming unequal variance for two-group comparisons or an ordinary one-way ANOVA with Tukey's test for multiple comparisons. In every case $P < .05$ was considered significant. * represents $P < .05$, ** $P < .01$, *** $P < .005$, **** $P < .001$ and ns not significant.

Results

Lactate and GSH Are the Most Significantly Reduced Metabolites Following TERT Silencing

First, we wanted to determine which ^{1}H-MRS-detectable intracellular metabolites were modulated by TERT in wild-type IDH GBM cells. We began by investigating the previously described genetically engineered NHARas/TERT cells, which serve as a model for GBM cells since they overexpress Ras and TERT.[31] We compared this model to cells in which the expression of TERT was silenced by treatment with two different TERT-targeting siRNAs. We confirmed that TERT expression was robustly reduced to comparable levels by both siRNAs (Supplementary Fig. S1A). A comparison of major metabolites in the ^{1}H spectra from NHARas/TERT cells treated with siCtrl and siTERT and a spectrum of NHARas/TERT siCtrl cells are illustrated in Figure 1A and Supplementary Fig. S1B.

Next, we performed an unsupervised PCA of the ^{1}H-MRS data comparing siCtrl and siTERT treatment groups. The PCA revealed a clear separation between groups (Figure 1B). Separation was also confirmed by OPLS-DA (Supplementary Fig. S1C) and the VIP score of each metabolite, derived from this analysis, revealed which metabolites were most important in contributing to the separation between TERT-expressing and nonexpressing cells. Lactate and GSH were identified as the topmost important metabolites (Figure 1C). The S line plot extracted from the OPLS-DA confirmed that these metabolites were the most significantly decreased following siTERT treatment (Supplementary Fig. S1D). The univariate analysis confirmed the significance of siTERT treatment-induced changes in lactate and GSH (Figure 1D) and other metabolites with VIP scores greater than 1 (Supplementary Fig. S2). This analysis supports the on-target effect of siTERT treatment as it showed no significant difference in the results obtained with the two siRNAs.

Because GABPB1 was recently identified as the upstream transcriptional factor binding to the mutant *TERT* promoter, we also wanted to assess the impact of TERT silencing by targeting GABPB1. NHA cells were engineered to overexpress TERT and thus do not have a mutant *TERT* promoter. We therefore next investigated the U87 human GBM cells, which do harbor *TERT* promoter mutations, and targeted TERT expression via siTERT or siGABPB1. The mRNA expression of TERT was suppressed by siTERT or siGABPB1 (Supplementary Fig. S3A). Multivariate and univariate analyses confirmed that with both treatments again GSH and lactate were the most significantly altered metabolites following TERT silencing. Furthermore, TERT

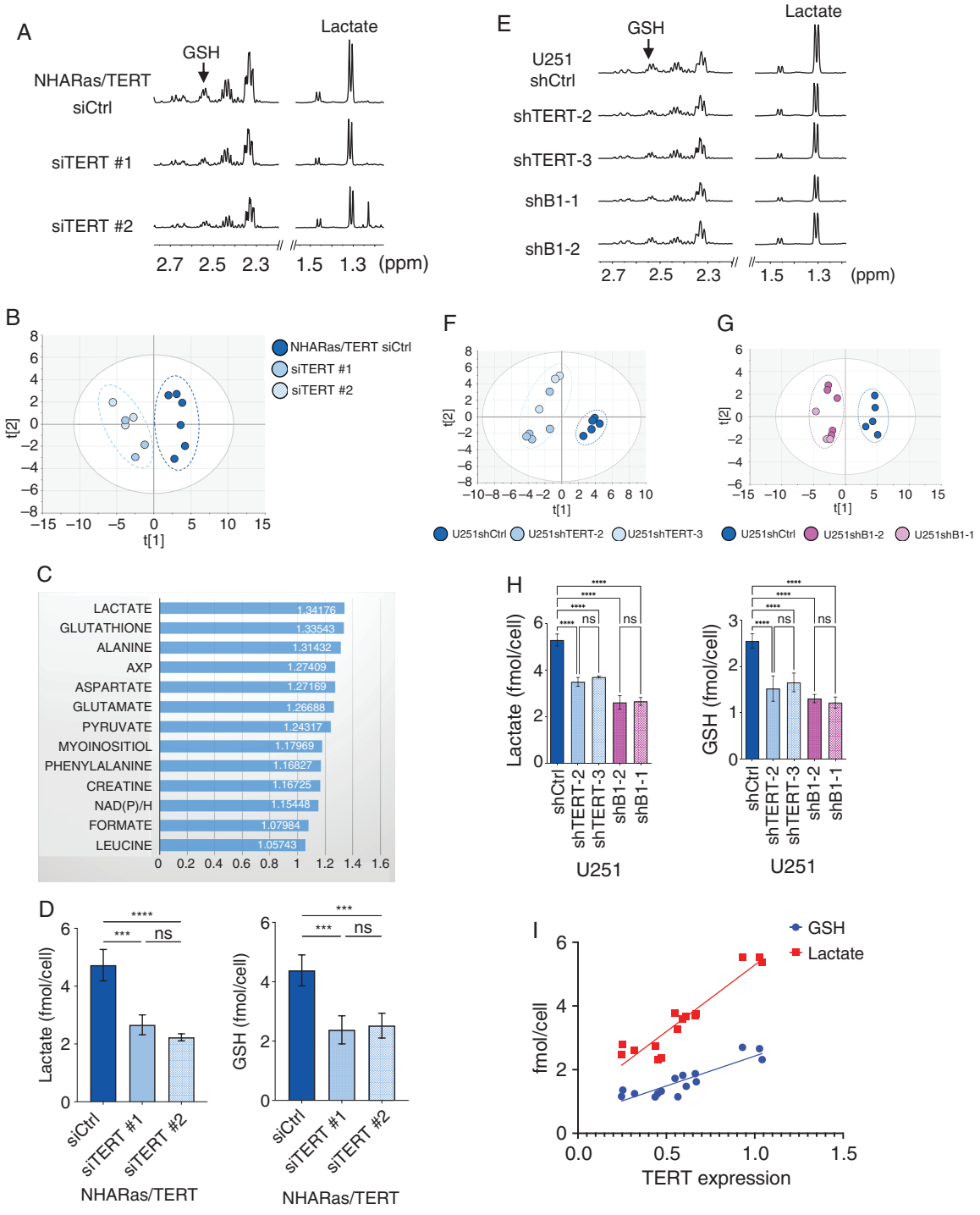

Fig. 1. Lactate and GSH are the most significantly reduced metabolites in multiple GBM models following TERT silencing. (A) Representative spectra of NHARas/TERT treated with siCtrl, siTERT #1, and siTERT #2 respectively. (B) PCA comparing siCtrl ($n = 6$) and siTERT ($n = 6$, siTERT #1 $n = 3$, siTERT #2 $n = 3$). t1 on x axis corresponds to PC1 and t2 on y axis corresponds to PC2. (C) VIP predictive scores derived from OPLS-DA, illustrating metabolites with a score >1. (D) Univariate analysis of lactate and GSH levels comparing siCtrl ($n = 6$), siTERT #1 ($n = 3$), and siTERT #2 ($n = 3$). (E) Representative spectra of U251 cell lines stably expressing shRNAs. (F) PCA comparing U251shCtrl ($n = 5$) and U251shTERT (U251shTERT-2 $n = 5$, U251shTERT-3 $n = 3$). t1 on x axis corresponds to PC1 and t2 on y axis corresponds to PC2. (G) PCA analysis comparing U251shCtrl ($n = 5$) and U251shB1 (U251shB1-2 $n = 5$, U251shB1-1 $n = 3$). t1 on x axis corresponds to PC1and t2 on y axis corresponds to PC2. (H) Univariate analysis of lactate and GSH levels comparing U251shCtrl ($n = 5$), U251shTERT-2 ($n = 5$), U251shTERT-3 ($n = 3$), U251shB1-2 ($n = 5$), and U251shB1-1 ($n = 3$). (I) GSH and lactate levels in U251shCtrl, U251shTERT, and U251shB1 cells as a function of TERT expression (GSH; $R^2 = 0.9007$, $P < .0001$, lactate; $R^2 = 0.9127$, $P < .0001$).

expression significantly correlated with GSH and lactate levels (Supplementary Table S4 and Supplementary Fig. S3B-D).

Next, we investigated the metabolism of the established human GBM cell line U251, which also harbors *TERT* promoter mutations. We compared these cells to their counterparts in which TERT was silenced by stable expression of shRNA targeting TERT or GABPB1. TERT expression was significantly reduced in both U251shTERT and U251shB1 cells compared to U251shCtrl and there was no significant difference in TERT expression between cells transduced with two different shRNAs targeting TERT or GABPB1 (Supplementary Fig. S4A).

Spectra comparing U251-based cells illustrated a reduction in lactate and GSH in U251shTERT and U251shB1 compared to U251shCtrl (Figure 1E). The PCA score plots comparing U251shCtrl and U251shTERT showed a clear separation between groups (Figure 1F) and this was confirmed by OPLS-DA (Supplementary Fig. S4B). As in the case of siRNA treatment, the VIP predictive scores revealed that lactate and GSH were the top two most important metabolites contributing to the separation between control and TERT-silenced cells (Supplementary Fig. S4C). The comparison of U251shCtrl and U251shB1 also revealed clear separation between groups (Figure 1G and Supplementary Fig. S4D) and VIP scores showed that again lactate and GSH were the top significantly reduced metabolites (Supplementary Fig. S4E). We confirmed the significance of the drop in lactate and GSH levels, and the comparable results with different TERT or GABPB1 shRNAs using univariate analysis (Figure 1H). Changes in other metabolites are illustrated in Supplementary Fig. S4F. Finally, we found a strong correlation between metabolite levels and TERT expression (Figure 1I) indicating that the metabolic changes in GSH and lactate are likely mediated by TERT independent of how its expression is silenced.

To further corroborate our findings, we performed studies using GBM1 and GS2, two additional patient-derived GBMs with *TERT* promoter mutations. TERT expression was reduced in GBM1shTERT and GBM1shB1 cells (Supplementary Fig. S5A) and spectra again showed a decrease in lactate and GSH (Supplementary Fig. S5B). As with other models, there was little difference in the metabolic changes observed between cells with different TERT or GABPB1-targeting shRNAs. Furthermore, the multivariate analysis, VIP scores, and univariate analysis confirmed that metabolism is altered by TERT silencing, and lactate and GSH levels were the most significantly reduced metabolites (Supplementary Table S5, Fig. S5C). Finally, again, we observed a strong correlation between TERT expression, GSH, and lactate (Supplementary Fig. S5D). Similar observations were made in the GS2 model (Supplementary Table S6, Fig. S6).

Finally, to confirm that our observations are associated with TERT, we silenced TERT or GABPB1 in a doxycycline-inducible manner in U251 cells. Doxycycline led to a drop in TERT expression and a proportionate decrease in lactate and GSH levels consistent with Figure 1I. TERT, lactate, and GSH were also rescued by doxycycline removal in both dox-inducible U251shTERT and dox-inducible U251shB1 (Supplementary Fig. S7).

TERT Silencing Is Associated With a Drop in Glycolytic and PPP Fluxes

In all our five human GBM models, the ^{1}H-MRS data pointed to lactate and GSH as the most significantly altered metabolites with TERT knockdown. In this study, we therefore further focused on these two metabolites and wanted to determine which underlying metabolic pathways were altered. To that end, we performed metabolic flux analysis using thermally-polarized [2-^{13}C]glucose, which provides information regarding fluxes via glycolysis and the pentose phosphate pathway (PPP; Figure 2A).[32]

Flux analysis for NHARas/TERT cells revealed that [2-^{13}C]lactate and [5-^{13}C]glutamate, associated with glycolysis, as well as [3-^{13}C]lactate and [4-^{13}C]glutamate, associated with the PPP, were all significantly reduced in siTERT-treated cells compared to siCtrl, indicating that both metabolic pathways were suppressed when TERT was silenced (Figure 2B). The results in the U251 model were similar. [2-^{13}C]lactate and [5-^{13}C]glutamate as well as [3-^{13}C]lactate and [4-^{13}C]glutamate were all significantly reduced indicating that both glycolysis and PPP were downregulated when TERT was silenced (Figure 2C).

We also determined the levels of NADPH, which is produced via the PPP and maintains reduced GSH, and found that TERT silencing in both the NHARas/TERT and U251 models resulted in a significant reduction in NADPH levels (Figure 2D and E), consistent with the reduction in PPP flux. NADH and NAD^{+} were also generally lower following TERT silencing, consistent with the ^{1}H-MRS (Supplementary Fig. S8A-F). ROS was significantly increased by TERT knockdown, in line with lower GSH and NADPH levels (Figure 2F and G).

TERT Silencing Is Associated with Alterations in Enzymes of Glycolytic and PPP Pathways

To determine the underlying mechanism for our findings, we investigated enzymes of the glycolytic and PPP pathways. We found that expression was downregulated with TERT-silencing in every case and most importantly in the case of known rate-limiting enzymes. In the glycolytic pathway, the expression of GLUT1, which is the main glucose importer, the expression and activity of lactate dehydrogenase A (LDHA), which controls lactate production, and the expression of MCT1 and MCT4, the major monocarboxylate transporters responsible for import and export of lactate and pyruvate, were all significantly reduced in NHARas/TERT cells compared to siCtrl-treated, and in U251shTERT and U251shB1 compared to U251shCtrl (Figure 3A–J). In the PPP, we found a reduction in the expression and activity of glucose-6-phosphate dehydrogenase (G6PD), the rate-limiting step of the pathway (Figure 3K–N). The expression of other major glycolytic and PPP was also lower when TERT was silenced (Supplementary Fig. S9). Our findings were confirmed with a small-scale RNAseq study (Supplementary Tables S7 and S8). Collectively, our data demonstrate that TERT silencing-induced downregulation of flux via glycolysis and the PPP is associated with modulation of expression of multiple enzymes, including, but not limited to, the rate-limiting enzymes of these pathways.

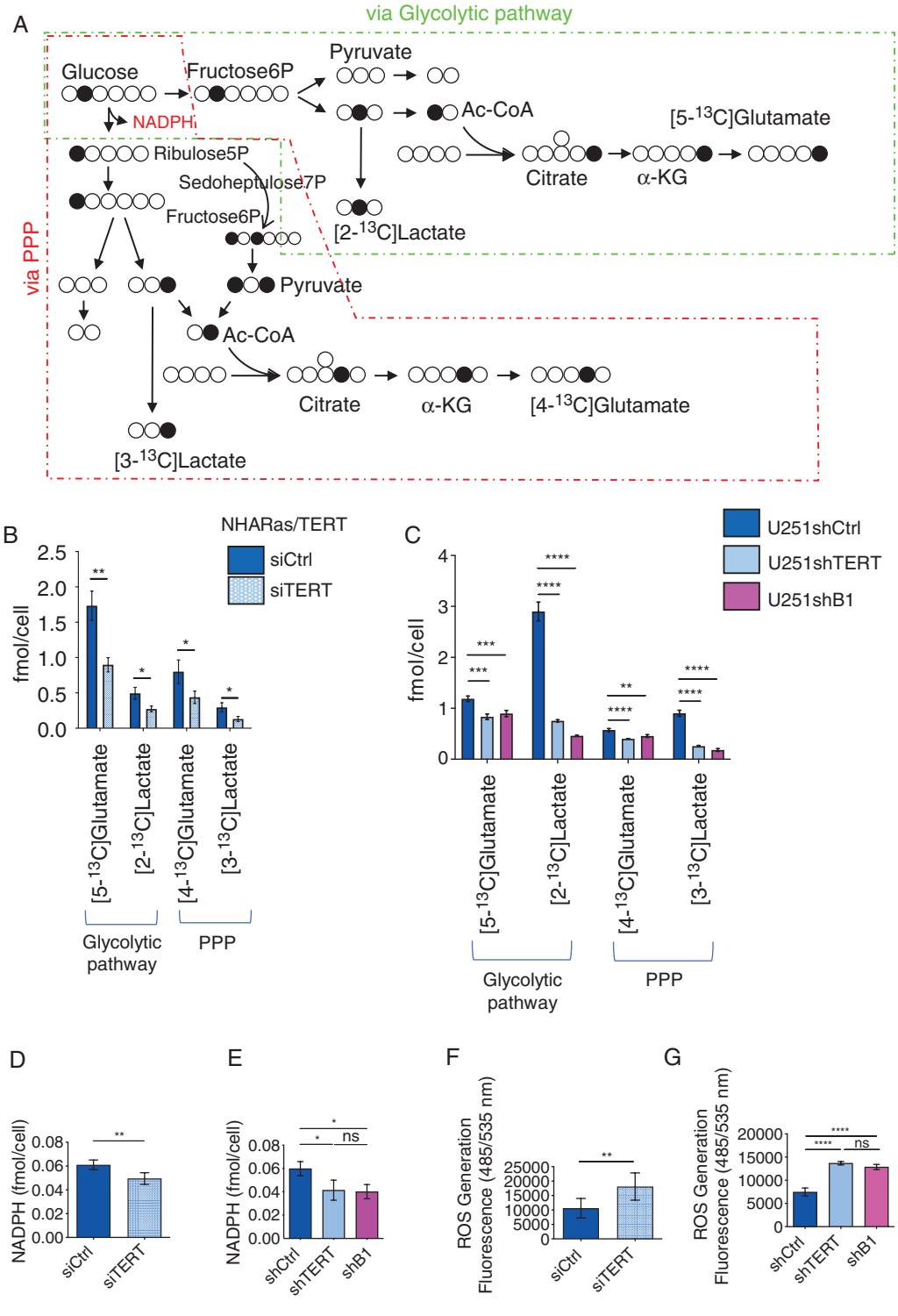

Fig. 2. TERT silencing is associated with a drop in glycolytic and PPP fluxes, as well as redox state. (A) Schema of metabolic pathways illustrating the fate of labeled carbons (black circles) from [2-^{13}C]glucose into the glycolytic pathway and TCA cycle or pentose phosphate pathway and TCA cycle. (B) Levels of [5-^{13}C]glutamate, [2-^{13}C]lactate, [4-^{13}C]glutamate, and [3-^{13}C]lactate comparing siCtrl and siTERT-treated NHARas/TERT cells. (C) Levels of [5-^{13}C]glutamate, [2-^{13}C]lactate, [4-^{13}C]glutamate, and [3-^{13}C]lactate comparing U251shCtrl, U251shTERT, and U251shB1 cells. (D) NADPH levels in NHARas/TERT cells treated with siCtrl and siTERT (n = 5, respectively). (E) NADPH levels in U251shCtrl, U251shTERT, and U251shB1 cells (n = 5, respectively). (F) ROS levels in siCtrl and siTERT-treated NHARas/TERT cells (n = 6, respectively). (G) ROS levels in U251shCtrl, U251shTERT, and U251shB1 cells (n = 3, respectively).

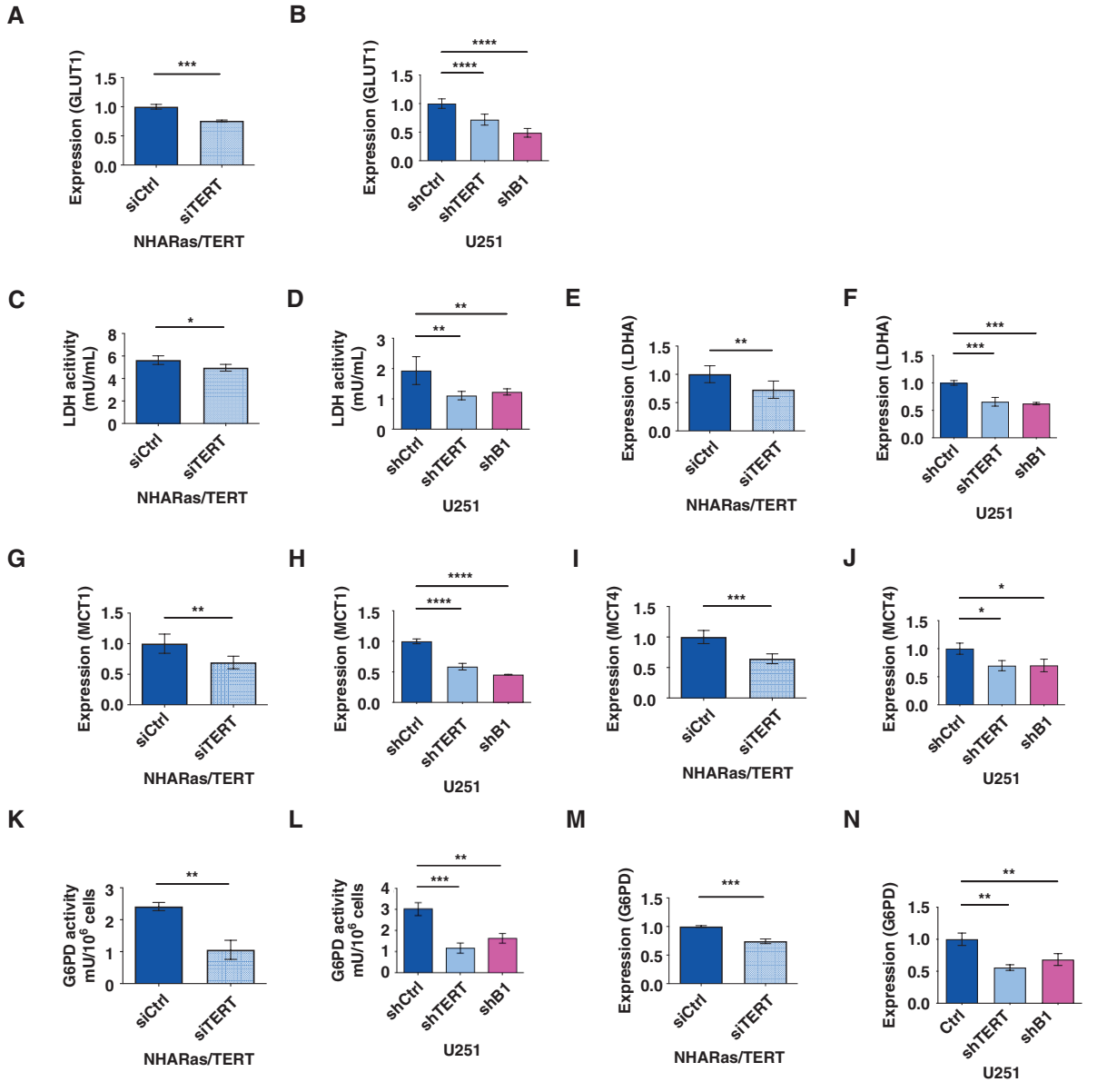

Fig. 3. TERT silencing is associated with alterations in enzymes of the glycolytic and PPP pathways. (A) Relative GLUT1 expression in NHARas/TERT cells treated with siCtrl and siTERT ($n = 3$, respectively). (B) Relative GLUT1 expression in U251shCtrl, U251shTERT, and U251shB1 cells ($n = 6$, respectively). (C) LDH activity in NHARas/TERT cells treated with siCtrl and siTERT ($n = 4$, respectively). (D) LDH activity in U251shCtrl, U251shTERT, and U251shB1 cells ($n = 5$, respectively). (E) Relative LDHA expression in NHARas/TERT cells treated with siCtrl and siTERT ($n = 5$, respectively). (F) Relative LDHA expression in U251shCtrl, U251shTERT, and U251shB1 cells ($n = 3$, respectively). (G) Relative MCT1 expression in NHARas/TERT cells treated with siCtrl and siTERT ($n = 5$, respectively). (H) Relative MCT1 expression in U251shCtrl, U251shTERT, and U251shB1 cells siTERT ($n = 5$, respectively). (I) Relative MCT4 expression in NHARas/TERT cells treated with siCtrl and siTERT ($n = 5$, respectively). (J) Relative MCT4 expression in U251shCtrl, U251shTERT, and U251shB1 cells ($n = 4$, respectively). (K) G6PD activity in siCtrl and siTERT in NHARas/TERT cells ($n = 3$, respectively). (L) G6PD activity in U251shCtrl, U251shTERT, and U251shB1 cells ($n = 3$, respectively). (M) Relative G6PD expression in NHARas/TERT cells treated with siCtrl and siTERT ($n = 3$, respectively). (N) Relative G6PD expression in U251shCtrl, U251shTERT, and U251shB1 cells ($n = 3$, respectively).

TERT Silencing Leads to a Drop in Hyperpolarized [1-^{13}C]pyruvate Conversion to Lactate in Cells

Our results indicated that glycolysis and lactate production were down-regulated when TERT was silenced. We, therefore, questioned whether we could monitor this metabolic change using the clinically-translatable hyperpolarized ^{13}C-MRS method probing pyruvate conversion to lactate. A spectral array of NHARas/TERT cells following injection of hyperpolarized [1-^{13}C]pyruvate shows the production of [1-^{13}C]lactate (Figure 4A). The sum spectrum, temporal evolution, and quantification of the lactate-to-pyruvate ratio

(Figure 4B–D) illustrate the drop in hyperpolarized [1-^{13}C]lactate production following siTERT treatment.

To confirm those results, we performed the same study in the U251 model. The spectral array of U251shCtrl cells demonstrates the production of [1-^{13}C]lactate and the sum spectrum illustrates the decrease in [1-^{13}C]lactate in both U251shTERT and U251shB1 (Supplementary Fig. S10). As in the case of the NHARas/TERT model, the lactate-to-pyruvate ratio was also significantly lower when TERT was silenced (Figure 4E and F). Similar findings were observed in the GS2 and GBM1 models (Supplementary Fig. S11A-D).

In Vivo ^{1}H-MRS Confirmed That Lactate and GSH Are Biomarkers of TERT

To assess the translational value of our findings, we next evaluated the ^{1}H-MRS-detectable metabolic differences that are observed in vivo when comparing U251shCtrl, U251shTERT, and U251shB1 tumors in rat brains. Figure 5A illustrates tumor volume over time. Consistent with TERT silencing, U251shTERT and U251shB1 tumors grew slower than U251shCtrls (Figure 5A). ^{1}H-MRS spectra were recorded when a 4 × 4 × 4 mm^3 voxel could be placed within the tumor region: day 28 ± 2 or 35 ± 2 postimplantation for U251shCtrl tumors and day 42 ± 2 for U251shTERT and U251shB1. Spectra and T_2-weighted images of tumor-bearing and normal brains are presented in Figure 5B and Supplementary Fig. S12A-C. Consistent with the cell results, LCModel quantification of the metabolites showed that both GSH and the composite lactate plus lipid signals were significantly lower in U251shTERT or U251shB1 tumors compared to U251shCtrl tumors (Figure 5C and D). Compared to normal brain, metabolite levels were higher in U251shTERT and U251shB1 tumors likely due to incomplete silencing of TERT expression in those cells.

In Vivo ^{13}C-MRS Demonstrated That Hyperpolarized Lactate Is a Reliable Biomarker of TERT

To assess the translational value of our hyperpolarized studies, we investigated the in vivo fate of hyperpolarized [1-^{13}C]pyruvate in U251shCtrl, U251shTERT, and U251shB1 tumors. ^{13}C-MRS spectra following injection of hyperpolarized [1-^{13}C]pyruvate show clearly detectable levels of [1-^{13}C]lactate, [1-^{13}C]pyruvate-hydrate, and [1-^{13}C]pyruvate (Figure 6A). The temporal evolution of hyperpolarized [1-^{13}C]lactate illustrated in the form of a heat map demonstrates that lactate production is lower in the TERT-silenced U251shTERT and U251shB1 tumors compared to the TERT-expressing U251shCtrl, and barely detectable in normal brain (Figure 6B). Data from the contralateral and normal brains were comparable (Supplementary Fig. S13). Quantification of the dynamic lactate-to-pyruvate ratio (Figure 6C and D) showed that, as expected, the difference between tumor and contralateral brain, and tumor and normal brain was significant. Also, similar to our ^{1}H-MRS findings, [1-^{13}C]lactate production in TERT-silenced tumors remained higher than in the contralateral brain and normal brain, likely reflecting residual TERT expression. Nonetheless, and most importantly, we found that the difference in hyperpolarized lactate production between the TERT-expressing and TERT-silenced tumors was significant, confirming the value of hyperpolarized lactate as a biomarker of TERT.

Discussion

Our first key finding when assessing the impact of TERT silencing was that lactate and GSH were consistently the topmost significantly altered ^{1}H-MRS-detectable metabolites and that their cellular levels were correlated with TERT expression. The drop in lactate can be readily explained by the reduced expression of glycolytic enzymes including the glucose transporter and LDHA. This finding is also consistent with previous work that showed that TERT knockdown attenuated glycolysis and the Warburg effect via the downregulation of glucose uptake and glycolytic enzymes.[33–35] The change in GSH can be explained by the drop in PPP enzymes including G6PD. It is also in line with prior reports that TERT translocates to the mitochondria and increases GSH levels to control reactive oxygen species, and supports the idea that TERT has extratelomeric roles.[36] The modulation of GSH is also consistent with prior studies from our lab in mutant IDH1 glioma models, wherein GSH levels were higher in TERT-expressing cells compared to controls.[20] In contrast, however, our prior work in mutant IDH1 cells showed no changes in lactate levels. Indeed, lactate production is generally low in mutant IDH1 lower-grade glioma models as a result of LDHA silencing[37] likely explaining the different findings in mutant and wild type IDH1 glioma. Nonetheless, it is worth noting that the other metabolites associated with TERT expression in mutant IDH1 cells, namely NAD(P)/H, aspartate, and AXP, were all among the metabolites significantly reduced when TERT was silenced in this study. Collectively, our investigations, therefore, point to a potentially common set of metabolic changes that are associated with TERT in all glioma and glioblastoma cells, with additional metabolic alterations such as lactate reflecting the combination of TERT with other oncogenic events associated with gliomagenesis.

^{1}H-MRS informs only on steady-state metabolite levels, and lactate is known to accumulate in areas of necrosis. Probing the dynamic production of lactate, in addition to its steady-state levels, can therefore provide important complementary information regarding changes in metabolism that are associated with TERT modulation. A second key finding of this study is that this information can be obtained using ^{13}C-MRS to monitor the conversion of hyperpolarized [1-^{13}C]pyruvate to lactate. In all our models, TERT silencing resulted in a reduction in hyperpolarized lactate production from pyruvate. The drop in hyperpolarized lactate can result from several metabolic events including reduced expression of monocarboxylate transporters that import pyruvate into the cell, reduced activity of LDHA that mediates lactate production, lower NADH, the cofactor for LDHA, or reduced steady-state lactate levels.[38,39] Following TERT silencing, we have found that all of these factors are altered in our GBM models providing a mechanistic explanation of our findings and validating our results.

Our final key finding is that the reduction in GSH, lactate, and hyperpolarized lactate occurs independently of

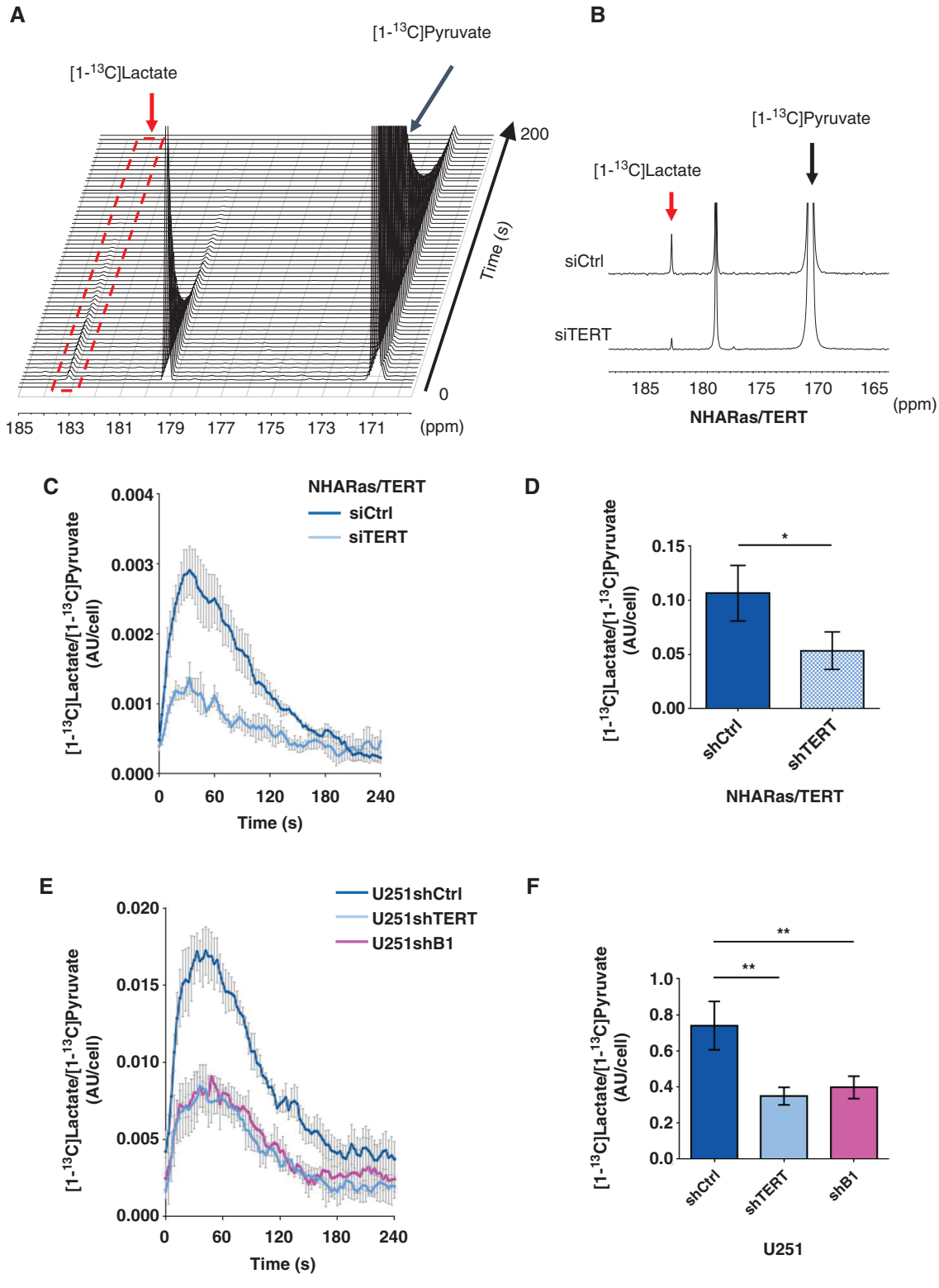

Fig. 4. TERT silencing leads to a drop in hyperpolarized [1-^{13}C]pyruvate conversion to lactate in live cells. (A) Spectral array of 13C spectra following [1-13C]pyruvate injection into NHARas/TERT cells treated with siCtrl. (B) Sum of the spectra comparing siCtrl and siTERT-treated NHARas/TERT cells. (C) Temporal evolution of [1-13C]lactate/[1-13C]pyruvate comparing siCtrl and siTERT-treated NHARas/TERT cells ($n = 4$, respectively). (D) The AUC of [1-13C]lactate/[1-13C]pyruvate comparing siCtrl and siTERT-treated NHARas/TERT cells ($n = 4$, respectively). (E) Temporal evolution of [1-13C]lactate/[1-13C]pyruvate comparing U251shCtrl, U251shTERT, and U251shB1 ($n = 5, 3, 3$, respectively). (F) The AUC of [1-^{13}C]lactate/[1-^{13}C]pyruvate comparing U251shCtrl, U251shTERT, and U251shB1 ($n = 5, 3, 3$, respectively).

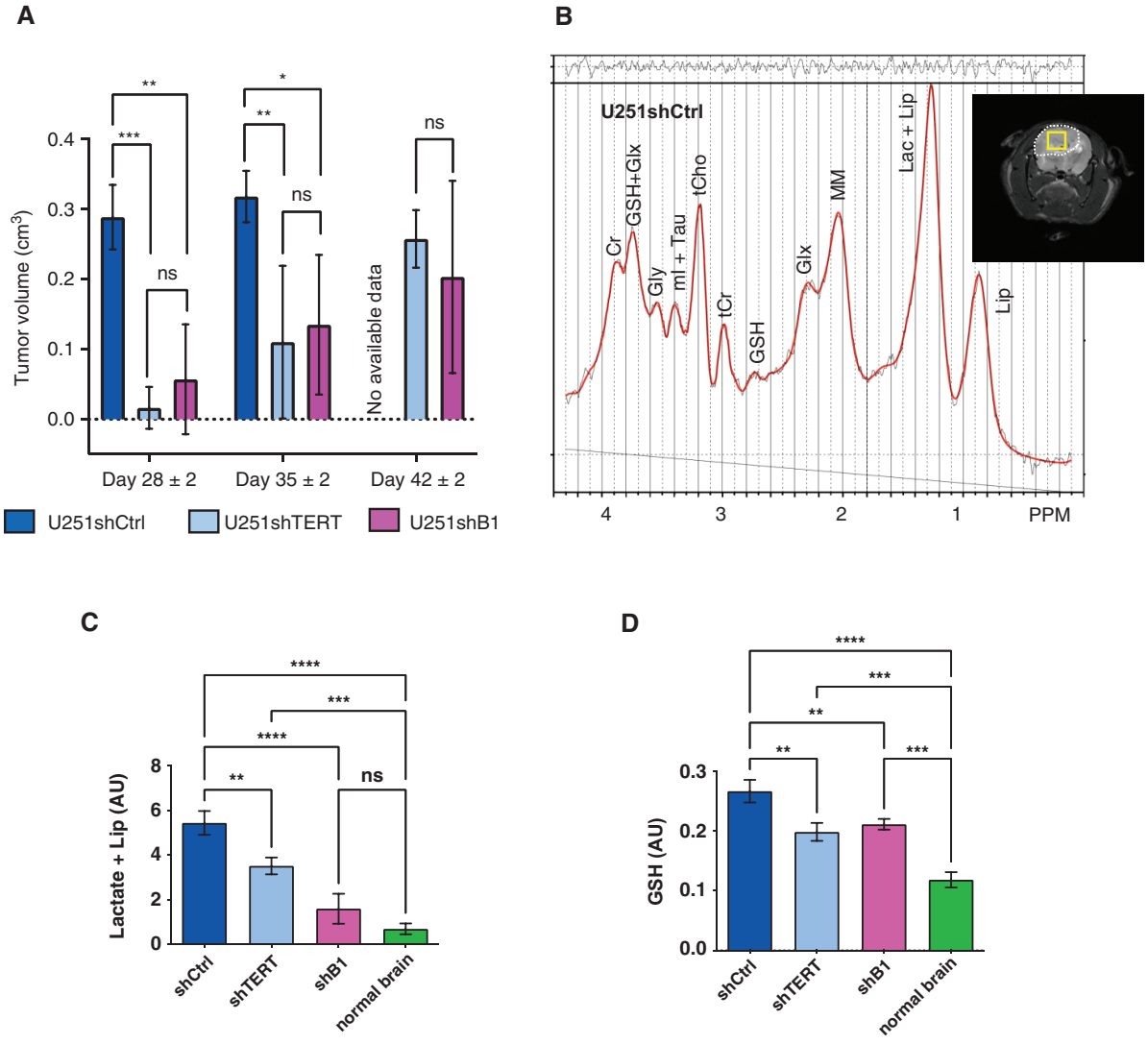

Fig. 5. In vivo ^{1}H MRS confirms that changes in lactate and GSH are associated with TERT silencing in glioblastoma. (A) Tumor volume change post-implantation comparing U251shCtrl, U251shTERT, and U251shB1 (Day28 ± 2 $n = 3, 4, 3$, Day35 ± 2 $n = 3, 4, 3$, Day42 ± 2 $n = 0, 3, 3$). The number of animals in U251Ctrl and U251shTERT groups dropped on Day42 ± 2 due to tumor-induced animal loss. (B) Representative ^{1}H-MRS spectrum and T_2-weighted image (insert) of U251shCtrl tumor. The tumor is contoured in white and the spectroscopic voxel position is illustrated in yellow in the anatomic image. (C) Univariate analysis of the composite lactate plus lipid peak comparing U251shCtrl, U251shTERT, and U251shB1 tumors, and normal brain ($n = 3$, respectively). (D) Univariate analysis of GSH levels comparing U251shCtrl, U251shTERT, and U251shB1 ($n = 3$, respectively).

whether TERT expression is silenced via GABPB1 or directly via TERT targeting. Furthermore, most of the other significant ^{1}H-MRS-detectable metabolic changes were also common to the two TERT silencing approaches, albeit with different levels of importance. This similarity suggests that most of the metabolic changes might be mediated by TERT. To the best of our knowledge, this is the first MRS study describing the effect of GABPB1 on cellular metabolism or comparing the metabolic effects of TERT and GABPB1.

When considering clinical imaging, previous preclinical studies have reported on using positron emission tomography (PET) or radioactive antisense oligonucleotides to image TERT,[40] but, to date, no clinical studies that directly predict TERT expression by PET have been reported. Small-scale studies have used T_2-weighted, perfusion, and diffusion MRI images combined with radiomics and machine learning methods to distinguish IDH and *TERT* promoter status.[41,42] Whether such methods could also be used to detect the inhibition of TERT expression remains to be determined. Nonetheless, including our metabolic imaging biomarkers would likely enhance radiomics methods to monitor TERT status. Importantly, the MRS-detectable metabolic biomarkers identified in this preclinical study are highly translatable. The utility of ^{1}H-MRS in the clinic has been extensively demonstrated, and dedicated sequences to monitor lactate and GSH have been implemented in brain tumor patients.[16] The translation of hyperpolarized pyruvate to

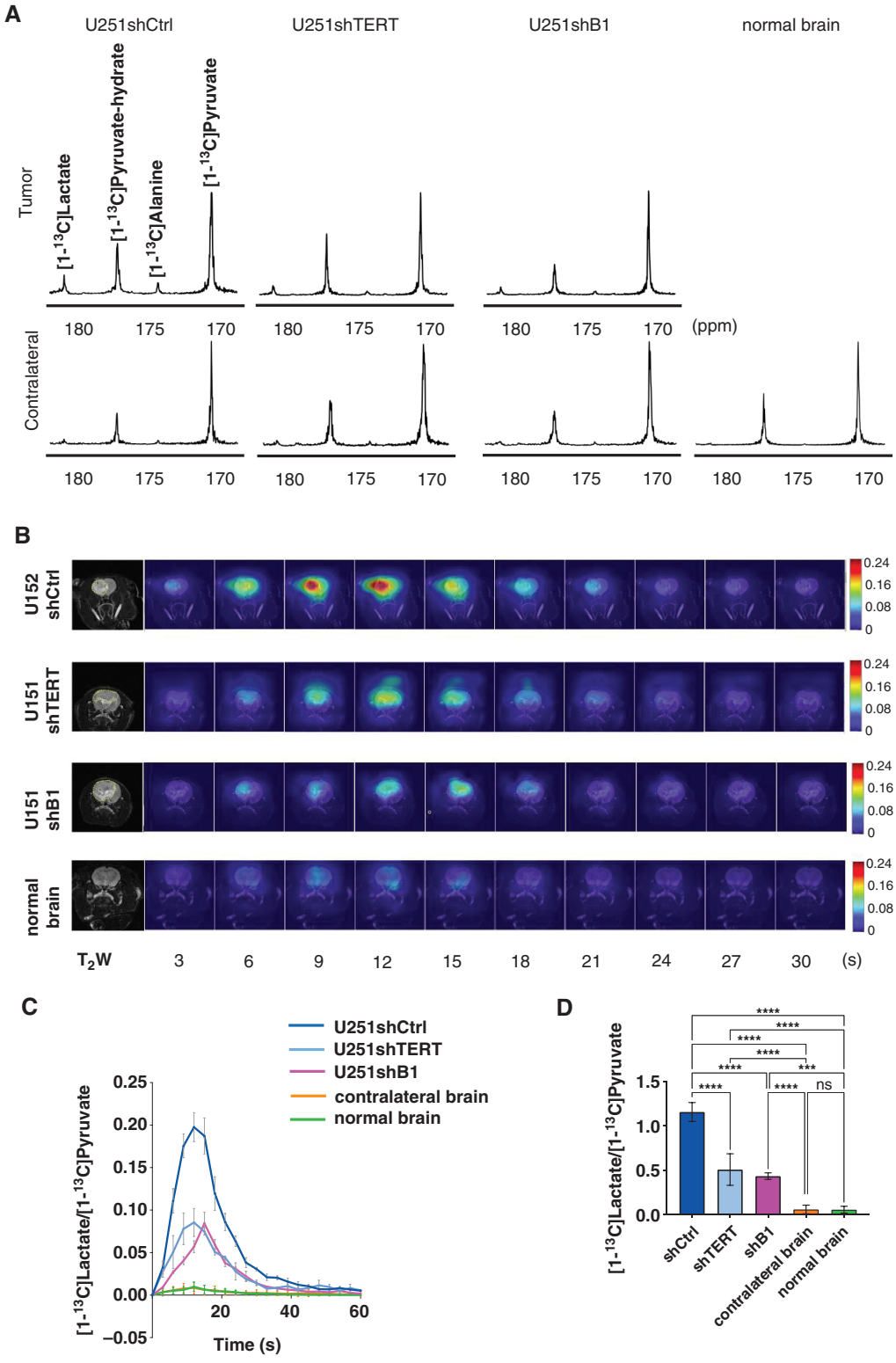

Fig. 6. In vivo ^{13}C-MRS of hyperpolarized pyruvate metabolism confirms that a drop in hyperpolarized lactate production is associated with TERT silencing in glioblastoma. (A) Representative ^{13}C spectra from each tumor model at 12 s after injection of hyperpolarized [1-^{13}C]pyruvate. (B) Dynamic hyperpolarized ^{13}C EPSI data of [1-^{13}C]lactate acquired from one slice from each tumor model at 3 s temporal resolution. (C) Average dynamic lactate to pyruvate ratio of tumor voxel from each tumor model, contralateral brain and normal brain (n = 4, 3, 3, 9, 3, respectively). (D) AUC of [1-^{13}C]lactate/[1-^{13}C]pyruvate comparing U251shCtrl, U251shTERT, U251shB1 tumors, contralateral brain, and normal brain (n = 4, 3, 3, 9, 3, respectively).

monitor metabolism in brain tumors has also been demonstrated.[43,44] Further studies will be needed to confirm the utility of MRS for monitoring response to emerging TERT-targeted therapeutics, but our results indicating that the MRS metabolic biomarkers can detect TERT silencing, are promising. This will be particularly important given our increasing understanding of the role of GABP in controlling TERT expression in mutant *TERT* promoter cells, and the role GABPB1 is expected to play as a tumor-specific therapeutic target.[7,8,10]

In summary, our study identified ^{1}H-MRS-detectable GSH and lactate, combined with ^{13}C-MRS-detectable hyperpolarized lactate, as metabolic biomarkers of TERT-targeted therapy for human GBM with *TERT* promoter mutations. These biomarkers could be translated to the clinic and thus improve the monitoring and personalized treatment of GBM patients.

Supplementary Material

Supplementary material is available at *Neuro-Oncology* online.

Keywords

glioblastoma | hyperpolarized ^{13}C-MRS | imaging biomarkers | magnetic resonance spectroscopy, (MRS) | metabolism

Funding

This work was supported by National Institutes of Health (NIH) R01CA172845, NIH R01CA197254, NIH P01CA118816, UCSF LOGLIO collective, UCSF NICO project, NIH P30CA082103, NIH R01CA239288, NIH K00CA212470, and Department of Defense W81XWH201055315. The authors also acknowledge support from NIH P41EB013598.

Conflict of interest statement. J. Costello is a co-founder of Telo Therapeutics Inc. and has an ownership interest. All other authors have no potential conflict of interest.

Authorship statement. N.M. and D.H. were involved in the study design, performed experiments, analyzed and interpreted data, and wrote the manuscript. N.S. generated all shRNA transduced cell lines and reviewed the manuscript. C.B. generated and screened shRNA constructs and reviewed the manuscript. M.R., Y.K., G.B., and A.M.G. helped perform experiments and reviewed the manuscript. C.H. and L.C. performed and analyzed RNAseq studies, R.O.P. and J.F.C. provided the cell models, helped with study design, reviewed and edited the manuscript. P.V. helped with study design, reviewed and edited the manuscript. S.M.R. designed the study, reviewed experiments, reviewed and edited the manuscript. All authors have read and agreed to the submitted version of the manuscript.

References

1. Maciejowski J, de Lange T. Telomeres in cancer: tumour suppression and genome instability. *Nat Rev Mol Cell Biol.* 2017; 18(3):175–186.
2. Killela PJ, Reitman ZJ, Jiao Y, et al. TERT promoter mutations occur frequently in gliomas and a subset of tumors derived from cells with low rates of self-renewal. *Proc Natl Acad Sci USA.* 2013; 110(15):6021–6026.
3. Vinagre J, Almeida A, Populo H, et al. Frequency of TERT promoter mutations in human cancers. *Nat Commun.* 2013; 4:2185.
4. Arita H, Narita Y, Fukushima S, et al. Upregulating mutations in the TERT promoter commonly occur in adult malignant gliomas and are strongly associated with total 1p19q loss. *Acta Neuropathol.* 2013; 126(2):267–276.
5. Korber V, Yang J, Barah P, et al. Evolutionary trajectories of IDH(WT) glioblastomas reveal a common path of early tumorigenesis instigated years ahead of initial diagnosis. *Cancer Cell.* 2019; 35(4):692–704.e12.
6. Chiappori AA, Kolevska T, Spigel DR, et al. A randomized phase II study of the telomerase inhibitor imetelstat as maintenance therapy for advanced non-small-cell lung cancer. *Ann Oncol.* 2015; 26(2):354–362.
7. Amen AM, Fellmann C, Soczek KM, et al. Cancer-specific loss of TERT activation sensitizes glioblastoma to DNA damage. *Proc Natl Acad Sci USA.* 2021; 118(13):e2008772118.
8. Bell RJ, Rube HT, Kreig A, et al. Cancer. The transcription factor GABP selectively binds and activates the mutant TERT promoter in cancer. *Science.* 2015; 348(6238):1036–1039.
9. Bell RJ, Rube HT, Xavier-Magalhaes A, et al. Understanding TERT promoter mutations: a common path to immortality. *Mol Cancer Res.* 2016; 14(4):315–323.
10. Mancini A, Xavier-Magalhaes A, Woods WS, et al. Disruption of the beta1L isoform of GABP reverses glioblastoma replicative immortality in a TERT promoter mutation-dependent manner. *Cancer Cell.* 2018; 34(3):513–528.e8.
11. Diplas BH, Liu H, Yang R, et al. Sensitive and rapid detection of TERT promoter and IDH mutations in diffuse gliomas. *Neuro Oncol.* 2019; 21(4):440–450.
12. Ellingson BM, Bendszus M, Boxerman J, et al. Consensus recommendations for a standardized Brain Tumor Imaging Protocol in clinical trials. *Neuro Oncol.* 2015; 17(9):1188–1198.
13. Viswanath P, Chaumeil MM, Ronen SM. Molecular imaging of metabolic reprograming in mutant IDH cells. *Front Oncol.* 2016; 6:60.
14. Suh CH, Kim HS, Jung SC, Choi CG, Kim SJ. 2-Hydroxyglutarate MR spectroscopy for prediction of isocitrate dehydrogenase mutant glioma: a systemic review and meta-analysis using individual patient data. *Neuro Oncol.* 2018; 20(12):1573–1583.
15. Gillies RJ, Morse DL. In vivo magnetic resonance spectroscopy in cancer. *Annu Rev Biomed Eng.* 2005; 7:287–326.
16. Li Y, Park I, Nelson SJ. Imaging tumor metabolism using in vivo magnetic resonance spectroscopy. *Cancer J.* 2015; 21(2):123–128.
17. Kurhanewicz J, Vigneron DB, Ardenkjaer-Larsen JH, et al. Hyperpolarized (13)C MRI: path to clinical translation in oncology. *Neoplasia.* 2019; 21(1):1–16.
18. Kurhanewicz J, Vigneron DB, Brindle K, et al. Analysis of cancer metabolism by imaging hyperpolarized nuclei: prospects for translation to clinical research. *Neoplasia.* 2011; 13(2):81–97.

19. Park I, Larson PEZ, Gordon JW, et al. Development of methods and feasibility of using hyperpolarized carbon-13 imaging data for evaluating brain metabolism in patient studies. *Magn Reson Med.* 2018; 80(3):864–873.
20. Viswanath P, Batsios G, Ayyappan V, et al. Metabolic imaging detects elevated glucose flux through the pentose phosphate pathway associated with TERT expression in low-grade gliomas. *Neuro Oncol.* 2021;23(9):1509–1522.
21. Viswanath P, Batsios G, Mukherjee J, et al. Non-invasive assessment of telomere maintenance mechanisms in brain tumors. *Nat Commun.* 2021; 12(1):92.
22. Ohba S, Mukherjee J, Johannessen TC, et al. Mutant IDH1 expression drives TERT promoter reactivation as part of the cellular transformation process. *Cancer Res.* 2016; 76(22):6680–6689.
23. Ronen SM, Jackson LE, Beloueche M, Leach MO. Magnetic resonance detects changes in phosphocholine associated with Ras activation and inhibition in NIH 3T3 cells. *Br J Cancer.* 2001; 84(5):691–696.
24. Izquierdo-Garcia JL, Viswanath P, Eriksson P, et al. Metabolic reprogramming in mutant IDH1 glioma cells. *PLoS One.* 2015; 10(2):e0118781.
25. Subramani E, Radoul M, Najac C, et al. Glutamate is a noninvasive metabolic biomarker of IDH1-mutant glioma response to temozolomide treatment. *Cancer Res.* 2020; 80(22):5098–5108.
26. Chaumeil MM, Radoul M, Najac C, et al. Hyperpolarized (13)C MR imaging detects no lactate production in mutant IDH1 gliomas: Implications for diagnosis and response monitoring. *Neuroimage Clin.* 2016; 12:180–189.
27. Nelson SJ. Analysis of volume MRI and MR spectroscopic imaging data for the evaluation of patients with brain tumors. *Magn Reson Med.* 2001; 46(2):228–239.
28. Provencher SW. Estimation of metabolite concentrations from localized in vivo proton NMR spectra. *Magn Reson Med.* 1993; 30(6):672–679.
29. Yen YF, Kohler SJ, Chen AP, et al. Imaging considerations for in vivo 13C metabolic mapping using hyperpolarized 13C-pyruvate. *Magn Reson Med.* 2009; 62(1):1–10.
30. Chen HY, Autry AW, Brender JR, et al. Tensor image enhancement and optimal multichannel receiver combination analyses for human hyperpolarized (13) C MRSI. *Magn Reson Med.* 2020; 84(6):3351–3365.
31. Sonoda Y, Ozawa T, Hirose Y, et al. Formation of intracranial tumors by genetically modified human astrocytes defines four pathways critical in the development of human anaplastic astrocytoma. *Cancer Res.* 2001; 61(13):4956–4960.
32. Brekke EM, Walls AB, Schousboe A, Waagepetersen HS, Sonnewald U. Quantitative importance of the pentose phosphate pathway determined by incorporation of 13C from [2-13C]- and [3-13C]glucose into TCA cycle intermediates and neurotransmitter amino acids in functionally intact neurons. *J Cereb Blood Flow Metab.* 2012; 32(9):1788–1799.
33. Bagheri S, Nosrati M, Li S, et al. Genes and pathways downstream of telomerase in melanoma metastasis. *Proc Natl Acad Sci USA.* 2006; 103(30):11306–11311.
34. Li S, Crothers J, Haqq CM, Blackburn EH. Cellular and gene expression responses involved in the rapid growth inhibition of human cancer cells by RNA interference-mediated depletion of telomerase RNA. *J Biol Chem.* 2005; 280(25):23709–23717.
35. Shaheen F, Grammatopoulos DK, Muller J, Zammit VA, Lehnert H. Extra-nuclear telomerase reverse transcriptase (TERT) regulates glucose transport in skeletal muscle cells. *Biochim Biophys Acta.* 2014; 1842(9):1762–1769.
36. Saretzki G. Extra-telomeric functions of human telomerase: cancer, mitochondria and oxidative stress. *Curr Pharm Des.* 2014; 20(41):6386–6403.
37. Chesnelong C, Chaumeil MM, Blough MD, et al. Lactate dehydrogenase A silencing in IDH mutant gliomas. *Neuro Oncol.* 2014; 16(5):686–695.
38. Dafni H, Larson PEZ, Hu S, et al. Hyperpolarized ^{13}C spectroscopic imaging informs on hypoxia-inducible factor-1 and Myc activity downstream of platelet-derived growth factor receptor. *Cancer Res.* 2010; 70(19):7400–7410.
39. Rao Y, Gammon S, Zacharias NM, et al. Hyperpolarized [1-^{13}C]pyruvate-to-[1-^{13}C]lactate conversion is rate-limited by monocarboxylate transporter-1 in the plasma membrane. *Proc Natl Acad Sci USA.* 2020; 117(36):22378–22389.
40. Jung KO, Youn H, Kim SH, et al. A new fluorescence/PET probe for targeting intracellular human telomerase reverse transcriptase (hTERT) using Tat peptide-conjugated IgM. *Biochem Biophys Res Commun.* 2016; 477(3):483–489.
41. Arita H, Kinoshita M, Kawaguchi A, et al. Lesion location implemented magnetic resonance imaging radiomics for predicting IDH and TERT promoter mutations in grade II/III gliomas. *Sci Rep.* 2018; 8(1):11773.
42. Fukuma R, Yanagisawa T, Kinoshita M, et al. Prediction of IDH and TERT promoter mutations in low-grade glioma from magnetic resonance images using a convolutional neural network. *Sci Rep.* 2019; 9(1):20311.
43. Miloushev VZ, Granlund KL, Boltyanskiy R, et al. Metabolic Imaging of the human brain with hyperpolarized (13)C pyruvate demonstrates (13)C lactate production in brain tumor patients. *Cancer Res.* 2018; 78(14):3755–3760.
44. Park I, Larson PE, Zierhut ML, et al. Hyperpolarized 13C magnetic resonance metabolic imaging: application to brain tumors. *Neuro Oncol.* 2010; 12(2):133–144.